Effect of exchange on interband magneto-absorption in zero gap Hg 1-kMnkTe mixed crystals

Gérald Bastard, C. Rigaux, Y. Guldner, J. Mycielski, A. Mycielski

Classification
Physics Abstracts
71.70G — 78.20L

EFFECT OF EXCHANGE ON INTERBAND MAGNETO-ABSORPTION IN ZERO GAP $Hg_{1-k}Mn_kTe$ MIXED CRYSTALS

G. BASTARD, C. RIGAUX, Y. GULDNER, J. MYCIELSKI (*) and A. MYCIELSKI (**)

Groupe de Physique des Solides de l'Ecole Normale Supérieure,
24, rue Lhomond, 75231 Paris 05, France

(*Reçu le 25 juillet 1977, révisé le 22 septembre 1977, accepté le 29 septembre 1977*)

Résumé. — Des expériences de magnétoabsorption ont été effectuées, à 4,2 et 2 K, dans la région spectrale 220-370 meV, sur des alliages $Hg_{1-k}Mn_kTe$ de gap nul. L'évolution des spectres $\Gamma_6 \rightarrow \Gamma_8$ avec la température et la composition révèle d'importantes modifications dans les sous-niveaux de spin des bandes Γ_6 et Γ_8 dues aux interactions d'échange entre les porteurs mobiles et les électrons d localisés. L'interprétation théorique des spectres magnétooptiques obtenus sur des alliages de faible composition en Mn a été effectuée dans l'approximation du cristal virtuel et du champ moléculaire en incluant les interactions d'échange dans le formalisme du modèle de Pidgeon et Brown. En ajustant l'énergie des transitions $\Gamma_6 \rightarrow \Gamma_8$ aux données expérimentales, nous déterminons l'aimantation en fonction du champ magnétique, à 4,2 et 2 K, et nous évaluons les paramètres d'échange pour les niveaux Γ_6 et Γ_8. Le spectre des niveaux de Landau, établi à $k_H = 0$, pour des alliages de faible k ($k \leqslant 0{,}015$) montre l'existence d'une transition semimétal → semiconducteur induite par le champ magnétique.

Abstract. — Magnetoabsorption experiments have been performed at 4.2 and 2 K in the spectral region 220-370 meV, on zero gap $Hg_{1-k}Mn_kTe$ alloys. The temperature and the composition dependence of the $\Gamma_6 \rightarrow \Gamma_8$ spectrum provides evidence of striking modifications in the Γ_8 and Γ_6 spin sublevels due to exchange interactions between localized d electrons and mobile carriers. The theoretical interpretation of the magnetooptical spectra of alloys of low Mn composition is carried out, using the virtual crystal and the molecular field approximations, by including the s-d and p-d exchange interactions within the framework of the Pidgeon and Brown model. By a fitting procedure of the $\Gamma_6 \rightarrow \Gamma_8$ transitions energies, the magnetization is determined at 4.2 and 2 K as a function of the magnetic field and the exchange parameters for the Γ_6 and Γ_8 levels are evaluated. The Landau level energy spectrum established, at $k_H = 0$, for alloys of composition up to 1.5 % exhibits a SM → SC transition induced by the magnetic field.

1. **Introduction.** — In recent literature, there has been particular interest in zero and narrow gap semi-conductors formed from HgTe. Among them, the system $Hg_{1-k}Mn_kTe$ receives considerable attention, as it provides attractive materials for investigating exchange phenomena.

Despite the different crystallographic structures of HgTe (zinc blende) and MnTe (hexagonal NiAs), solid solutions of $Hg_{1-k}Mn_kTe$ are formed over the range of composition $k < 0.8$. Alloys of $k < 0.4$ crystallise in the zinc blende lattice [1] : the tellurium atoms are located on the sites of one of the fcc sublattices, whereas mercury and manganese atoms are more or less randomly distributed over the second fcc sublattice sites.

Similarly to the alloy systems formed from HgTe, the $Hg_{1-k}Mn_kTe$ system exhibits either an inverted band structure, like HgTe, or a semiconducting structure (Fig. 1). The semimetal → semiconductor transition resulting from the triple degeneracy of Γ_6 (s-type) and Γ_8 (p-type) states occur near the composition $k = 0.07$ at 4.2 K [2].

The peculiarities of these Mn compounds are connected with the presence of half-filled $3d^5$ shells of the Mn atoms. The d electrons tightly bound to the Mn^{2+} ions give rise to localized magnetic moments which may interact through exchange coupling with conduction and valence electrons in the s and p states. As the spin-dependent properties are drastically affected by these s-d and p-d interactions, magneto-optics is a useful technique to investigate the exchange

(*) Institute of Theoretical Physics, Warsaw University, 00-681 Warsaw, Poland.
(**) Institute of Physics, Polish Academy of Sciences, 02-668 Warsaw, Poland.

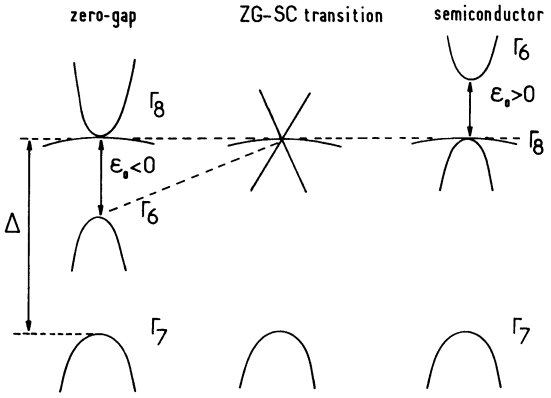

FIG. 1. — Band structure of $Hg_{1-k}Mn_kTe$ mixed crystals at the Γ point.

and localized spin ordering phenomena in zero and narrow gap $Hg_{1-k}Mn_kTe$ alloys.

Preliminary magnetooptical data have revealed anomalous electronic gyromagnetic factors in $Hg_{1-k}Mn_kTe$ of low $k \leqslant 0.02$ [2]. Magnetic susceptibility [3], (1), [13], helicon-spin-resonance [4] and EPR [5] measurements have shown that the effective localized spin behaves practically as if $L = 0$, $S = 5/2$ and $g_{Mn} = 2$. Alloys of low Mn composition are paramagnetic [3, 13].

We report experimental results of extensive magnetooptical studies performed on semimetallic $Hg_{1-k}Mn_kTe$ alloys of composition $k < 0.015$. $\Gamma_6 \rightarrow \Gamma_8$ interband magnetooptical transitions were investigated by magnetoabsorption experiments performed in the IR region 220-370 meV, with circularly and linearly polarized radiation. Magnetooptical spectra are described in section 3, with emphasis on the dominant features connected with the composition and temperature dependence. A theoretical model is developed in section 4, which describes the Landau levels in the Γ_8, Γ_6, Γ_7 states. Using the virtual crystal approximation, magnetic levels are obtained by including the exchange interactions within the framework of the Pidgeon and Brown [6] model. We use the molecular field approximation in treating the carrier-manganese exchange interaction. Fitting of magnetoabsorption data (section 5) provides a very sensitive method of determining the average spin orientation of manganese, even at very low manganese concentration. From the comparison between theory and experiments, band and exchange parameters are obtained. Γ_8 Landau levels are described, and the specific properties induced by the exchange interactions are analysed (sections 6 and 7).

2. **Experiments.** — $\Gamma_6 \rightarrow \Gamma_8$ transitions were investigated by magnetoabsorption experiments performed at low temperature on zero gap $Hg_{1-k}Mn_kTe$ of low Mn composition ($k \leqslant 1.5\,\%$).

(1) Galazka, R., private communication.

The mixed crystals were grown by a modified Bridgman method providing ingots of high homogeneity. The Mn molar content was determined for all investigated alloys by density measurements. The results are corroborated by electron microprobe analysis performed on several samples. The alloys were annealed under a saturated atmosphere of mercury to reduce the density of mercury vacancies. In all investigated alloys the position of the Fermi level lies close to the Γ_8 point. The thin samples required for transmission experiments were prepared by mechanical polishing and chemical etching in bromine methanol solution. Magnetotransmission spectra were obtained at 4 and 2 K, at fixed photon energies in the spectral region 220-370 meV, and with the applied magnetic field varying up to 55 kG. The incident electromagnetic radiation was linearly polarized along the magnetic field ($\boldsymbol{\varepsilon} /\!/ \mathbf{H} /\!/ z$) in the Voigt geometry, and circularly polarized (σ^+, σ^-) in the Faraday configuration, to select the magnetooptical transitions induced by each component ε_z, ε^+, ε^-

$$\varepsilon^{\pm} = \frac{\varepsilon_x \pm i\varepsilon_y}{\sqrt{2}}$$

of the electric field radiation.

3. **Experimental results.** — To illustrate the magnetooptical data obtained on alloys of low Mn composition, we present results, at 4.2 and 2 K, for five samples, with k varying from 0.001 to 0.015. The characteristics of the alloys are indicated in table I.

TABLE I

Samples	k	ε_0 (meV) at 4.2 K
—	—	—
A	0.001	− 293
B	0.004	− 277
C	0.008	− 249
D	0.0104	− 232
E	0.0150	− 200

The typical magnetotransmission spectrum (sample E), reported in figure 2, shows pronounced oscillations emphasizing the weak broadening of the Landau levels in these alloys. Figures 3-12 show the magnetic field dependence of the transition energies, at $T = 4.2$ and 2 K, for the different samples. From the region of convergence at vanishing magnetic field of the $\Gamma_6 \rightarrow \Gamma_8$ transition energies, the interaction gap $\varepsilon_0 = E_{\Gamma_6} - E_{\Gamma_8}$ is determined for each alloy. $\varepsilon_0(k)$, shown in figure 13, exhibits a linear variation in this range of composition.

The most striking features of the experiments consist in a strong temperature dependence of the spectra between 4.2 and 2 K, and also in a drastic modification in the relative positions of the lines with

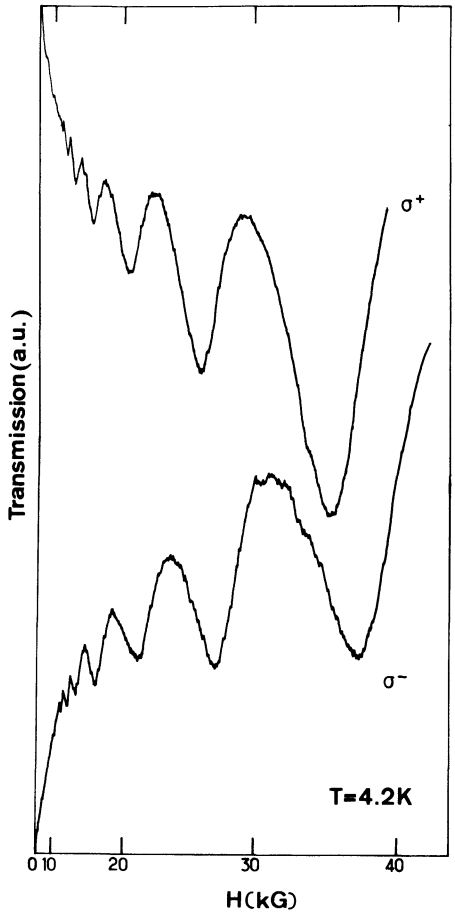

FIG. 2. — Magnetotransmission spectrum of sample E at the photon energy $\hbar\omega = 296.1$ meV. Faraday configuration. Circular polarization $T = 4.2$ K.

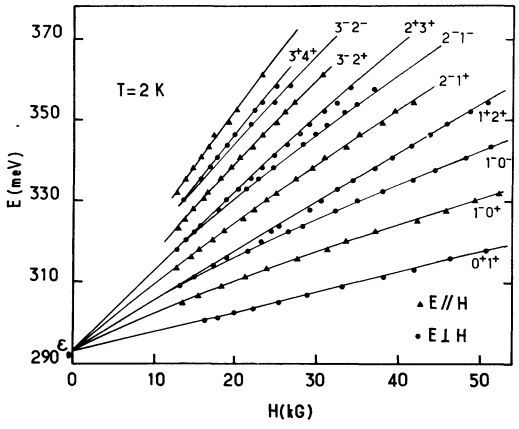

FIG. 4. — Magnetic field dependence of the $\Gamma_6 \rightarrow \Gamma_8$ transition energies. Sample A. $T = 2$ K. Solid lines : theory. Symbols : experiments.

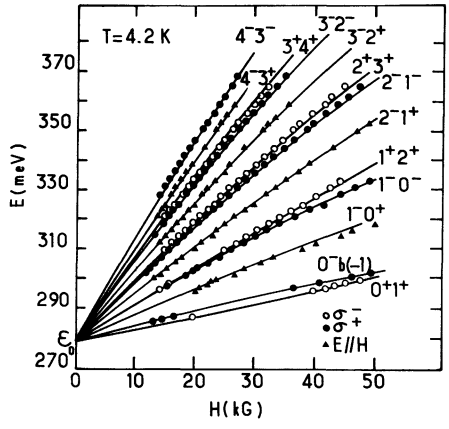

FIG. 5. — Magnetic field dependence of the $\Gamma_6 \rightarrow \Gamma_8$ transition energies. Sample B. $T = 4.2$ K. Solid lines : theory. Symbols : experiments.

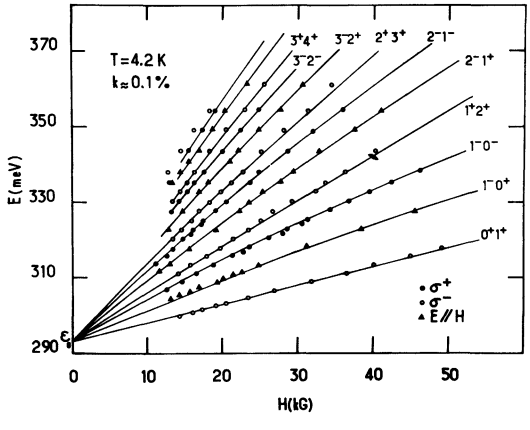

FIG. 3. — Magnetic field dependence of the $\Gamma_6 \rightarrow \Gamma_8$ transition energies sample A. $T = 4.2$ K. Solid lines : theory. Symbols : experiments.

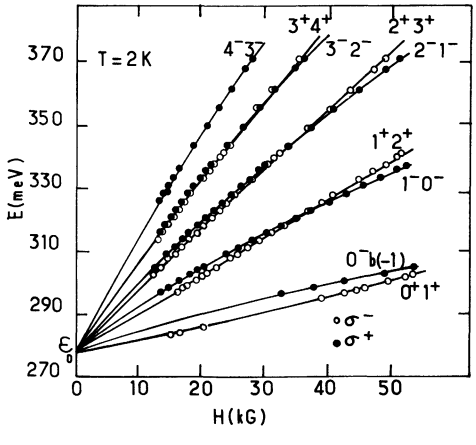

FIG. 6. — Magnetic field dependence of the $\Gamma_6 \rightarrow \Gamma_8$ transition energies. Sample B. $T = 2$ K. (Circular polarization.) Solid lines : theory. Symbols : experiments.

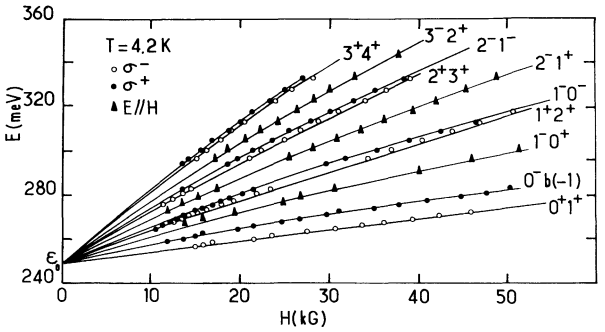

FIG. 7. — Magnetic field dependence of the $\Gamma_6 \rightarrow \Gamma_8$ transition energies. Sample C. $T = 4.2$ K. Solid lines : theory. Symbols : experiments.

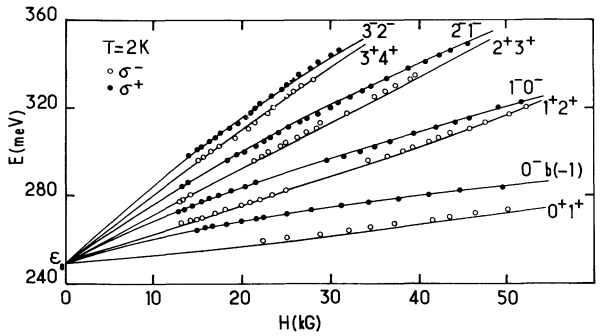

FIG. 8. — Magnetic field dependence of the $\Gamma_6 \rightarrow \Gamma_8$ transition energies. Sample C. $T = 2$ K. (Circular polarization.) Solid lines : theory. Symbols : experiments.

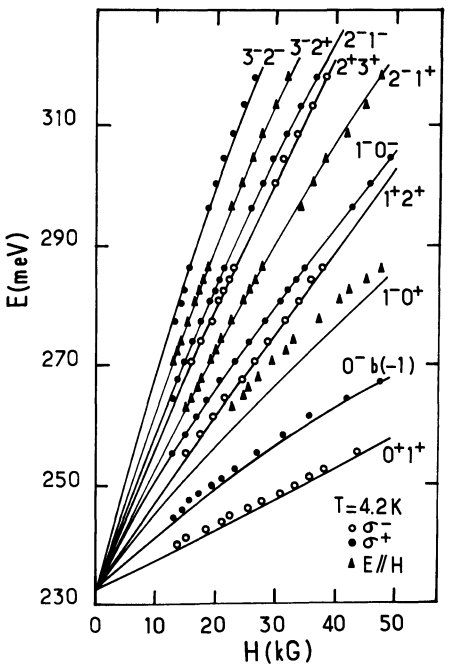

FIG. 9. — Magnetic field dependence of the $\Gamma_6 \rightarrow \Gamma_8$ transition energies. Sample D. $T = 4.2$ K. Solid lines : theory. Symbols : experiments.

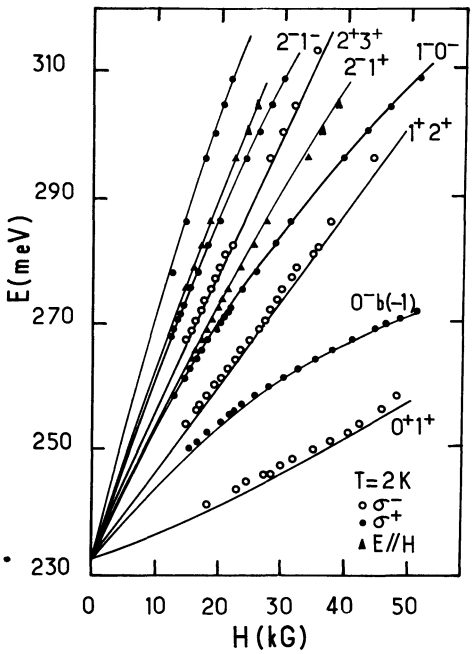

FIG. 10. — Magnetic field dependence of the $\Gamma_6 \rightarrow \Gamma_8$ transition energies. Sample D. $T = 2$ K. Solid lines : theory. Symbols : experiments.

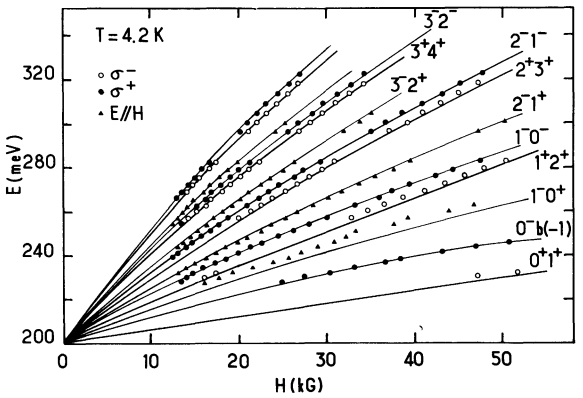

FIG. 11. — Magnetic field dependence of the $\Gamma_6 \rightarrow \Gamma_8$ transition energies. Sample E. $T = 4.2$ K. Solid lines : theory. Symbols : experiments.

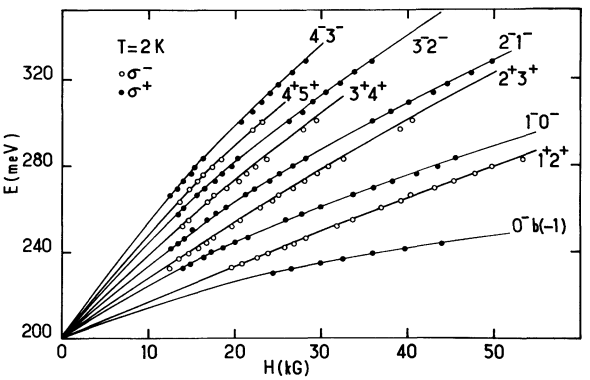

FIG. 12. — Magnetic field dependence of the $\Gamma_6 \rightarrow \Gamma_8$ transition energies. Sample E. $T = 2$ K. (Circular polarization.) Solid lines : theory. Symbols : experiments.

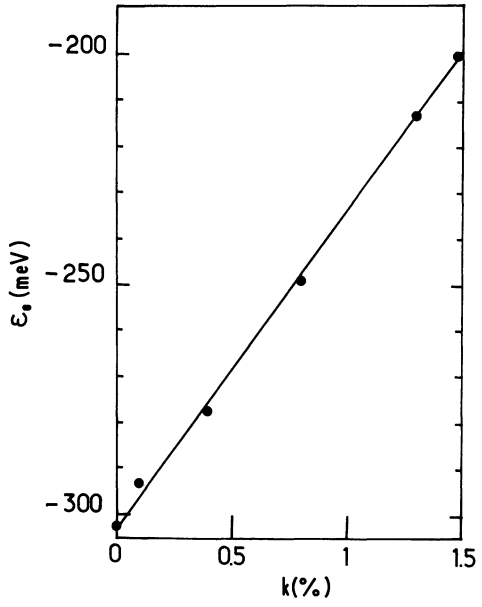

FIG. 13. — Composition dependence of the interaction gap. $T = 4.2$ K.

increasing Mn composition at fixed temperature. Both phenomena will be shown to be a consequence of the modification of the energies of the spin sublevels in Γ_6 and Γ_8 resulting from the exchange interactions of mobile carriers with the localized electrons. The reference to HgTe and the $Hg_{1-x}Cd_xTe$ alloys of comparable band structure, is crucial in unambiguously identifying the transitions and thereby in specifying the Landau level energy spectrum.

The selection rules [7, 8] for the dominant $\Gamma_6 \rightarrow \Gamma_8$ transitions are given in table II.

TABLE II

σ^+	$b_{\Gamma_6}(n+1) \rightarrow b_{\Gamma_8}(n)$	$(n+1)^- \rightarrow n^-$
σ^-	$a_{\Gamma_6}(n) \rightarrow a_{\Gamma_8}(n+1)$	$n^+ \rightarrow (n+1)^+$
$\varepsilon /\!/ \mathbf{H}$	$b_{\Gamma_6}(n+1) \rightarrow a_{\Gamma_8}(n)$	$(n+1)^- \rightarrow n^+$
Nomenclature	Pidgeon and Brown model [6]	Three band model [9] (2)

Comparing the spectra of $Hg_{1-x}Cd_xTe$ and $Hg_{1-k}Mn_kTe$ alloys of similar interaction gaps, at 4.2 K it can been seen that the transitions $\varepsilon /\!/ \mathbf{H}$ are nearly coincident whereas the positions of circular polarization lines, at each field, are shifted towards lower (for σ^-) or higher (for σ^+) energies with respect to the spectrum observed in $Hg_{1-x}Cd_xTe$ alloys [7]. This behaviour reflects an increase of the electronic spin splitting

$$S_c(n) = b_{\Gamma_8}(n) - a_{\Gamma_8}(n) :$$

we directly determine $S_c(n)$ from the energy distance between the transitions

$$b_{\Gamma_6}(n+1) \rightarrow b_{\Gamma_8}(n) \quad (\sigma^+)$$

and

$$b_{\Gamma_6}(n+1) \rightarrow a_{\Gamma_8}(n) \quad (\varepsilon /\!/ \mathbf{H}) .$$

(2) Nomenclature used in the figures.

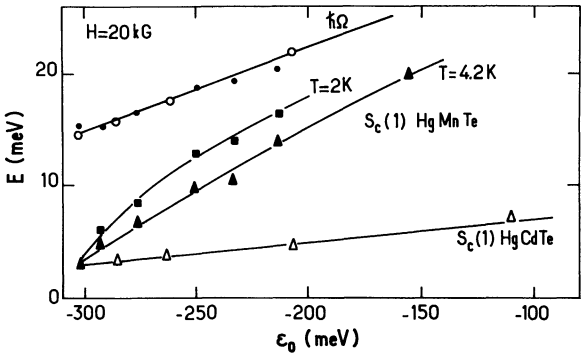

FIG. 14. — $S_c(1)$ and $\hbar\Omega$ as a function of ε_0 in HgCdTe (open symbols) and HgMnTe (black symbols) at $T = 4.2$ K and 2 K. $H = 20$ kG.

Figure 14 shows $S_c(1)$ as a function of ε_0, for both alloys systems, at $H = 20$ kG. We also report in figure 14 the energy distance $\hbar\Omega$ between adjacent transitions in the series σ^-. $\hbar\Omega$ (representing in the parabolic limit the sum of the cyclotron energies in Γ_6 and Γ_8 (conduction) bands) has comparable values for both systems of alloys $Hg_{1-x}Cd_xTe$ and $Hg_{1-k}Mn_kTe$, which shows the similarity of the effective mass parameters. The enhancement of $S_c(1)$ provides evidence of a modification of the electron spin sublevels in the $Hg_{1-k}Mn_kTe$ mixed crystals.

3.1 COMPOSITION DEPENDENCE OF THE MAGNETO-OPTICAL SPECTRA ($T = 4.2$ K). — Starting from HgTe, we follow continuously the evolution of the $\Gamma_6 \rightarrow \Gamma_8$ spectrum with gradually increasing Mn composition, which enables us to unambiguously identify the transitions. For the lowest content (sample A), the results are very similar to the spectrum observed in HgTe [10], in particular the transitions excited by σ^-, σ^+ and $\varepsilon /\!/ \mathbf{H}$ radiation components have the same ordering (Fig. 3). As k increases, the relative positions of the transition σ^+ and σ^- become drastically modified : the relative position of the paire of lines

$$a_{\Gamma_6}(n) \rightarrow a_{\Gamma_8}(n+1) \quad (\sigma^-)$$

and

$$b_{\Gamma_6}(n) \rightarrow b_{\Gamma_8}(n-1) \quad (\sigma^+)$$

is inverted as k varies from 0.001 (Fig. 3) to 0.008 (Fig. 7) and for $k = 0.004$ (Fig. 5) both lines are almost coincident. To illustrate the evolution of the circular polarization spectra, we plot in figure 15 the energy distance δ, at $H = 20$ kG, between $a_{\Gamma_6}(1) \rightarrow a_{\Gamma_8}(2)$ (σ^-) and $b_{\Gamma_6}(1) \rightarrow b_{\Gamma_8}(0)$ (σ^+) transitions as a function of ε_0, that we compare the behaviour in $Hg_{1-x}Cd_xTe$ alloys. δ shows an opposite dependence in both series of alloys and exhibits a sign reversal near $\varepsilon_0 = -270$ meV in $Hg_{1-k}Mn_kTe$. Figure 16 describes the spin splitting $S_c(1)$ for alloys of various compositions as a function of the magnetic field. These results provide evidence for a large enhan-

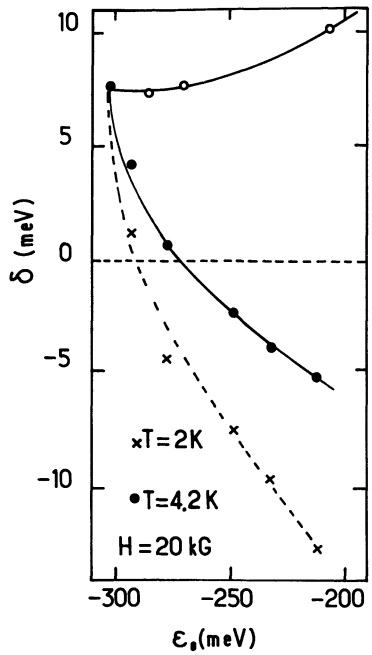

FIG. 15. — Energy distance between the transitions $a_{\Gamma_6}(1) \rightarrow a_{\Gamma_8}(2)$ (σ^-) and $b_{\Gamma_6}(1) \rightarrow b_{\Gamma_8}(0)$ (σ^+) as a function of ε_0 in HgCdTe (open circles) and HgMnTe. T = 4.2 and 2 K. H = 20 kG.

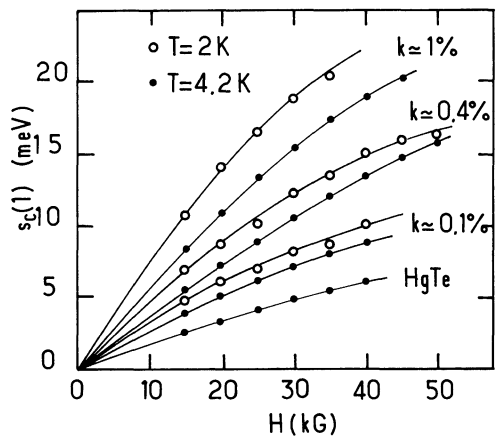

FIG. 16. — Spin splitting $S_c(1)$ of the n = 1 electronic level as a function of the magnetic field for HgTe and different $Hg_{1-k}Mn_kTe$ alloys. T = 4.2 K and 2 K.

cement of the electronic spin splitting with increasing k. Another experimental evidence of the strong modification of the $\Gamma_6 \rightarrow \Gamma_8$ spectrum is provided by the observation of a new transition for σ^+ polarization : this intense line exists in the spectra of alloys of composition $k \geqslant 0.004$ (Fig. 5, 7, 9, 11) and is unambiguously assigned to $b_{\Gamma_6}(0) \rightarrow b_{\Gamma_8}(-1)$, allowed for σ^+. The observation of this transition results from the emergence above the Fermi level of the hole Landau level $b_{\Gamma_8}(-1)$.

3.2 TEMPERATURE DEPENDENCE OF THE MAGNETO-OPTICAL SPECTRA. — In contrast with $Hg_{1-x}Cd_xTe$ alloys, the spectra of $Hg_{1-k}Mn_kTe$ exhibit a strong temperature dependence between 4 and 2 K, as shown in figures 3-12. The temperature decrease produces qualitatively comparable effects on the transition energies as in an increase of composition. By lowering T from 4.2 to 2 K, the spectrum $\varepsilon /\!/ \mathbf{H}$ is practically unaffected, whereas the lines associated with circular polarization are shifted towards higher (for σ^+) and lower (for σ^-) energies. The magnetotransmission spectra at 4.2 and 2 K for the samples C, B (Fig. 17, 18) show the shift (negative for σ^+ and positive for σ^-) of the resonance fields associated with $b_{\Gamma_6}(1) \rightarrow b_{\Gamma_8}(0)$, $b_{\Gamma_6}(0) \rightarrow b_{\Gamma_8}(-1)$ and $a_{\Gamma_6}(0) \rightarrow a_{\Gamma_8}(1)$ transitions.

This temperature behaviour implies an increase of the electronic spin splitting between 4.2 and 2 K, as shown in figure 16. Moreover, the curvatures of the

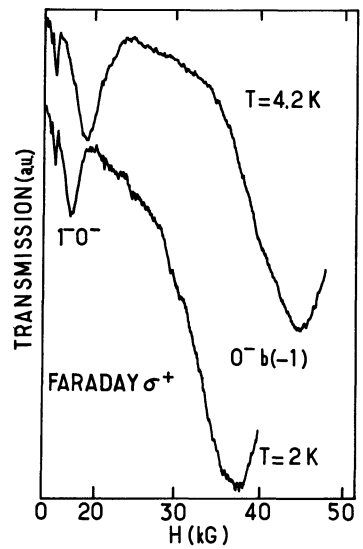

FIG. 17. — Magnetotransmission recordings at $\hbar\omega$ = 278.8 meV for sample C at T = 4.2 and 2 K. σ^+ polarization.

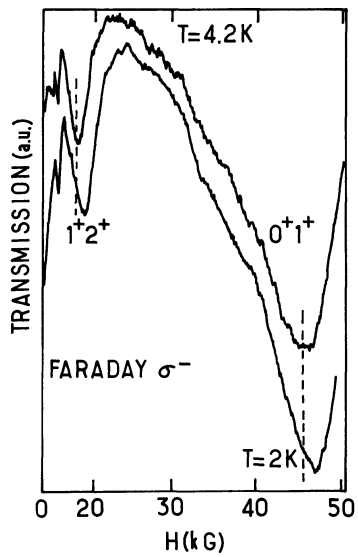

FIG. 18. — Magnetotransmission recordings at $\hbar\omega$ = 298,1 meV for sample B at T = 4.2 and 2 K. σ^- polarization.

circular polarization lines are accentuated with decreasing temperature. The diagrams $E(H)$ exhibit opposite curvatures for σ^+ and σ^- lines. At 2 K, the curves $E(H)$ are bent upwards (for σ^-) or downwards (for σ^+). This bowing effect, hardly visible at 4.2 K, is clearly observed at 2 K (Fig. 6, 8, 10, 12). It may give rise, for some particular composition, to a crossing of σ^+ and σ^- lines. For sample B (Fig. 6), the intersection of the pairs of lines $a_{\Gamma_6}(n) \rightarrow a_{\Gamma_8}(n+1)$ and $b_{\Gamma_6}(n) \rightarrow b_{\Gamma_8}(n-1)$ occurs in the investigated field range.

It should be pointed out that the temperature effects (displacement and curvatures of the lines) are more pronounced with increasing Mn content of the alloys.

From these experimental observations, one can conclude that the presence of the Mn atoms induces anomalous spin effects in the Γ_8 and Γ_6 Landau levels energy spectrum of the $Hg_{1-k}Mn_kTe$ mixed crystals, but do not significantly modify the band structure parameters with respect to the $Hg_{1-x}Cd_xTe$ system. Thus we ascribe the modification of the spin states to the exchange interactions between d electrons localized on the Mn atoms, and mobile carriers in Γ_8 and Γ_6 levels.

4. **Theoretical model.** — s and p electronic levels in random $Hg_{1-k}Mn_kTe$ alloys may be described within the virtual crystal approximation. The crystalline potential of the Hg and Mn atoms are replaced by the weighted average $\overline{V} = kV_{Mn} + (1-k)V_{Hg}$. Adding $\overline{V}$ to the Te atomic potential, the translational periodicity of the lattice is restored and the electrons are described in terms of Bloch states. The first order correction $\langle nk \mid V - \overline{V} \mid nk \rangle$ vanishes, and the deviations from the virtual crystal approximation lead only to a broadening of the levels. This approximation is meaningful only for outer shells of Hg and Mn atoms, i.e. for the $4s^2$(Mn) and $6s^2$(Hg) states from which originate the electronic states spatially extended over the crystal.

For deeper core states, such as the $3d^5$ electrons of the Mn atoms, which are tightly bound to the Mn^{2+} ions, the V.C.A. is irrelevant. These unfilled 3d shells will be described in terms of localized magnetic moments $\mathbf{S}_i$ ($S = 5/2$. $g_{Mn} = 2$).

In the presence of external magnetic field, the electronic states in s and p type bands are accurately described using the V.C.A. within the framework of the Pidgeon-Brown model [6]; Γ_6, Γ_8, Γ_7 Landau levels in small gap materials belonging to the zinc blende lattice are obtained by applying a procedure of nearly degenerate states. The closely spaced Γ_8, Γ_6, Γ_7 bands are treated exactly and the effects of higher bands upon the closely spaced states are accounted for up to order k^2. The Luttinger effects [11] in Γ_8 are included as well as the non parabolicity effects induced by the **k.p** interactions between s and p states. The magnetic levels in Γ_8, Γ_6, Γ_7 are the solutions of an 8 × 8 matrix Hamiltonian. If we neglect the inversion asymmetry and the anisotropy in Γ_8, the effective mass Hamiltonian D projected on the basis of the eight $u_j(J, M_J)$, ($j = 1, 2 \ldots 8$) band edges Bloch functions [6, 7] is given, at $k_z = 0$, by two 4 × 4 matrices D_a, D_b

$$D = \begin{pmatrix} D_a & 0 \\ 0 & D_b \end{pmatrix}.$$

In $Hg_{1-k}Mn_kTe$, the exchange interactions between s, p and d electrons should be accounted for. Kossut [14] has shown that these interactions can be described by the Heisenberg-type Hamiltonian

$$\mathcal{H}_{int} = \sum_{\mathbf{R}_i} J(\mathbf{r} - \mathbf{R}_i)\, \mathbf{S}_i . \boldsymbol{\sigma} . \qquad (1)$$

$\mathbf{S}_i$ represents a localized magnetic moment located at the site $\mathbf{R}_i$, $\boldsymbol{\sigma}$ is the mobile electron spin and $J(\mathbf{r} - \mathbf{R}_i)$ is an exchange integral centered at $\mathbf{R}_i$. Its spatial range, of atomic scale, is much smaller than the magnetic length λ. On the scale of the cyclotron radius, $J(\mathbf{r} - \mathbf{R}_i)$ can then be approximated by a contact interaction.

By accounting for the contact interaction, the introduction of $\mathcal{H}_{int}$ into the effective mass Hamiltonian introduces in D_a and D_b additional terms of the form :

$$\sum_i \mathbf{S}_i . \int_{cell} d\Omega u_{j1}^* \, J(\mathbf{r})\, \boldsymbol{\sigma} u_{j2} .$$

Using the explicit band edge Bloch functions [6, 7], the exchange contributions are expressed in terms of only two exchange parameters : $\alpha = \langle S \mid J(\mathbf{r}) \mid S \rangle$ and $\beta = \langle X \mid J(\mathbf{r}) \mid X \rangle$.

The manganese spin operators will be replaced by their thermodynamical average $\langle \mathbf{S}_i \rangle$. This corresponds to the standard molecular-field approximation in the theory of magnetism. It is very well justified in our case, as the mobile electron interacts simultaneously with an enormous number of manganese atoms.

For d electrons in $Hg_{1-k}Mn_kTe$ crystals, the thermodynamical average of the manganese spin operator along the applied magnetic field ($\mathbf{H} /\!/ z$) is

$$\langle S_i^z \rangle = - S f_{norm}(H, T)$$

where $S = 5/2$ and the transverse components vanish. $f_{norm}(H, T)$ denotes a normalized magnetization function. At low carrier concentrations ($n \sim 10^{15}$, $p \sim 10^{16}$ cm^{-3}), we can neglect the effect of carrier-manganese exchange interaction on the system of manganese spins. For non interacting manganese magnetic moments,

$$f_{norm}(H, T) = \frac{2}{5} B_{5/2}\left(\frac{g_{Mn}\, \mu_B\, H}{k_B\, T}\right)$$

where $B_{5/2}$ is the Brillouin function for a spin 5/2.

The addition of $\mathcal{H}_{int}$ to the effective mass Hamiltonian enables us to determine the Γ_6, Γ_8, Γ_7 Landau levels. Neglecting inversion asymmetry and anisotropy in Γ_8, the energy levels in the a and b ladders are the solutions of the determinantal eq. (2) and (3) respectively.

a set

$$\begin{bmatrix} \varepsilon_0+\hbar\omega_0(n+1)-\varepsilon_a(n)+3\,Ar & i\sqrt{n\frac{E_p}{2}\hbar\omega_0} & i\sqrt{(n+1)\frac{E_p}{6}\hbar\omega_0} & \sqrt{(n+1)\frac{E_p}{3}\hbar\omega_0} \\ -i\sqrt{n\frac{E_p}{2}\hbar\omega_0} & -\hbar\omega_0\left[(\gamma_1+\gamma)\left(n-\frac{1}{2}\right)+\frac{3}{2}\kappa\right] & -\hbar\omega_0\sqrt{3\,n(n+1)}\,\gamma & i\hbar\omega_0\sqrt{6\,n(n+1)}\,\gamma \\ & -\varepsilon_a(n)+3\,A & & \\ -i\sqrt{(n+1)\frac{E_p}{6}\hbar\omega_0} & -\hbar\omega_0\sqrt{3\,n(n+1)}\,\gamma & -\hbar\omega_0\left[(\gamma_1-\gamma)\left(n+\frac{3}{2}\right)-\frac{\kappa}{2}\right] & i\hbar\omega_0\sqrt{2}\left[\gamma\left(n+\frac{3}{2}\right)-\frac{\kappa+1}{2}\right] \\ & & -\varepsilon_a(n)-A & -2\sqrt{2}\,A \\ \sqrt{(n+1)\frac{E_p}{3}\hbar\omega_0} & -i\hbar\omega_0\,\gamma\sqrt{6\,n(n+1)} & -i\hbar\omega_0\sqrt{2}\left[\gamma\left(n+\frac{3}{2}\right)-\frac{\kappa+1}{2}\right] & -\hbar\omega_0\left[\gamma_1\left(n+\frac{3}{2}\right)-\left(\kappa+\frac{1}{2}\right)\right] \\ & & -2\sqrt{2}\,A & -A-\varepsilon_a(n)+A \end{bmatrix} = 0 \quad (2)$$

b set

$$\begin{bmatrix} \varepsilon_0+\hbar\omega_0\,n-\varepsilon_b(n)-3\,Ar & i\sqrt{n\frac{E_p}{6}\hbar\omega_0} & i\sqrt{(n+1)\frac{E_p}{2}\hbar\omega_0} & \sqrt{n\frac{E_p}{3}\hbar\omega_0} \\ -i\sqrt{n\frac{E_p}{6}\hbar\omega_0} & -\hbar\omega_0\left[(\gamma_1-\gamma)\left(n-\frac{1}{2}\right)+\frac{\kappa}{2}\right] & -\hbar\omega_0\,\gamma\sqrt{3\,n(n+1)} & i\hbar\omega_0\sqrt{2}\left[\gamma\left(n-\frac{1}{2}\right)+\frac{\kappa+1}{2}\right] \\ & -\varepsilon_b(n)+A & & +2\sqrt{2}\,A \\ -i\sqrt{(n+1)\frac{E_p}{2}\hbar\omega_0} & -\hbar\omega_0\,\gamma\sqrt{3\,n(n+1)} & -\hbar\omega_0\left[(\gamma_1+\gamma)\left(n+\frac{3}{2}\right)-\frac{3}{2}\kappa\right] & i\hbar\omega_0\,\gamma\sqrt{6\,n(n+1)} \\ & & -\varepsilon_b(n)-3\,A & \\ \sqrt{n\frac{E_p}{3}\hbar\omega_0} & -i\hbar\omega_0\sqrt{2}\left[\gamma\left(n-\frac{1}{2}\right)+\frac{\kappa}{2}+\frac{1}{2}\right] & -i\hbar\omega_0\,\gamma\sqrt{6\,n(n+1)} & -\hbar\omega_0\left[\gamma_1\left(n-\frac{1}{2}\right)+\kappa+\frac{1}{2}\right] \\ & +2\sqrt{2}\,A & & -A-\varepsilon_b(n)-A \end{bmatrix} = 0 \quad (3)$$

where $\hbar\omega_0$ is the free electron cyclotron energy.

$$A = -\frac{5}{12}\beta k N_0\, f_{\text{norm}}(H, T) \qquad (4)$$

r is the ratio α/β of the exchange integrals in Γ_6 and Γ_8 respectively. N_0 denotes the number of unit cells per unit volume.

The wavefunctions in the a and b Landau levels are given in terms of harmonic oscillator functions φ_n and band edges Bloch functions u_j [7] :

$$\psi_a(n) = \begin{bmatrix} a_{1n}\,\varphi_n \\ a_{3n}\,\varphi_{n-1} \\ a_{5n}\,\varphi_{n+1} \\ a_{7n}\,\varphi_{n+1} \end{bmatrix} \begin{matrix} \text{Basis} \\ u_1 \\ u_3 \\ u_5 \\ u_7 \end{matrix}; \qquad (5)$$

$$\psi_b(n) = \begin{bmatrix} b_{2n}\,\varphi_n \\ b_{4n}\,\varphi_{n-1} \\ b_{6n}\,\varphi_{n+1} \\ b_{8n}\,\varphi_{n-1} \end{bmatrix} \begin{matrix} \text{Basis} \\ u_2 \\ u_4 \\ u_6 \\ u_8 \end{matrix}. \qquad (6)$$

The solutions of eqs. (2, 3) are analytical only for the first ($n = -1$) quantum levels. The eigenvalues require numerical computations as a function of six band structure parameters (the interaction gap $\varepsilon_Q = E_{\Gamma_6} - E_{\Gamma_8}$, the spin orbit energy Δ, the Luttinger parameters γ_1, γ, κ describing the interaction between Γ_8 and higher bands and the Kane matrix element $E_p = 2/m_0 \mid \langle S \mid p_x \mid X \rangle \mid^2$), and two additional exchange parameters r and $A(H)$, depending on T and H through the magnetization functions.

5. **Comparison between theory and experiments.** — The quantitative analysis of the spectra is performed by using the theoretical description of Γ_8 and Γ_6 Landau levels given in section 4. $\Gamma_6 \to \Gamma_8$ magneto-optical transitions occur at $k_z = 0$ due to the singularities of the joint density of states. The exchange interactions do not change the explicit form of the wavefunction, which implies the conservation of the selection rules for $\Gamma_6 \to \Gamma_8$ transitions [7] (Table II). The dominant transitions are :

$$\begin{aligned} a_{\Gamma_6}(n) &\to a_{\Gamma_8}(n+1) \quad \sigma^- \\ b_{\Gamma_6}(n+1) &\to b_{\Gamma_8}(n) \quad \sigma^+ \\ b_{\Gamma_6}(n+1) &\to a_{\Gamma_8}(n) \quad \varepsilon /\!\!/ \mathbf{H}\,. \end{aligned} \qquad (7)$$

The transition energies were numerically fitted with the experimental lines according to the identification given in figures (3.12).

We applied a minimization procedure, at fixed magnetic field, of the sum

$$\sum = \sum_j | E_{ex}^j - E_{th}^j |^2$$

of the squared distance between experimental and theoretical energies where j runs over all transitions. By taking $\Delta = 1$ eV and the values of the Luttinger parameters $\gamma_1 = 3$, $\gamma = 0$, $\kappa = -1.65$ obtained for $Hg_{1-x}Cd_xTe$ [7] of low x, we restrict the variables to E_p, r and A, which are determined at each field by the minimization of $\sum$. For each alloy, E_p is relatively stable. In the investigated range of composition, E_p is found between 18.3 and 18.8 eV in excellent agreement with the results obtained in $Hg_{1-x}Cd_xTe$[7], which exemplifies the close similarity of the band structure in both alloy systems. The quality of the fit is almost insensitive to r between -0.55 and -0.45. By selecting the adequate value of E_p for each composition, and taking $r = -0.49$ for all samples, we determine the magnetization $A(H)$ as a function of the field by the minimization procedure. The normalized magnetization.

$$f_{norm}(H, T) = -\frac{12}{5}\frac{A(H, T)}{\beta k N_0} \qquad (8)$$

is then deduced. The k values in (8) are determined from the experimental values of ε_0 and $\varepsilon_0(k)$ (Fig. (13)).

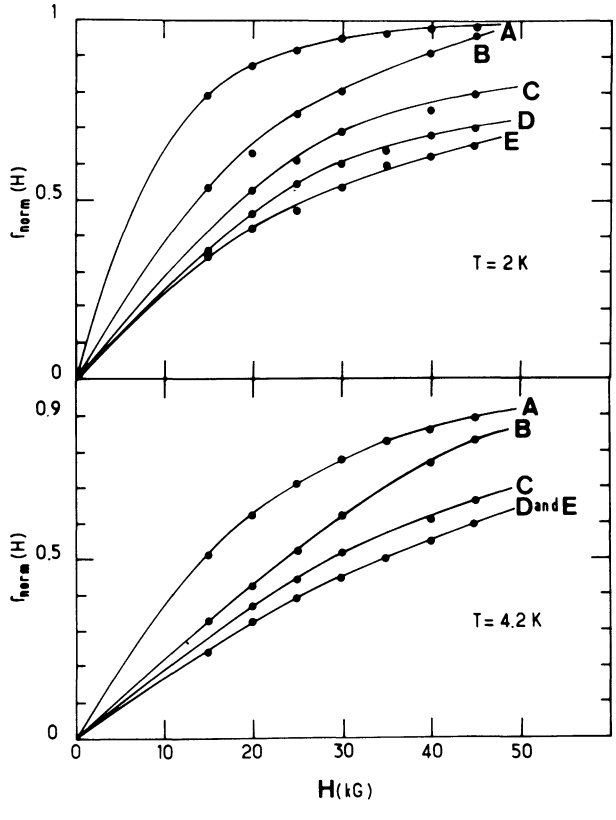

FIG. 19. — Magnetic field dependence of the normalized magnetization function at $T = 4.2$ and 2 K for the different alloys.

This relation was obtained from a least square fitting of the experimental data on ε_0 and k.

Figure 19 shows the field dependence of the normalized magnetization at $T = 4.2$ and 2 K. The results are in good agreement with direct magnetization measurements performed at 4.2 K on an $Hg_{1-k}Mn_kTe$ alloy of $k \simeq 0.01$ ([1]).

For the lowest Mn composition ($k = 0.0014$), f_{norm} follows the Brillouin law $B_{5/2}$. For higher Mn content, $f_{norm}(H, T)$ markedly differs from the Brillouin function and the deviations from the ideal model of non interacting localized spins are emphasized with increasing k.

The model of non interacting manganese spins cannot quantitatively account for the magnetization $f_{norm}(H)$ deduced from our experiments. The measured dependence of the average manganese spin orientation shows a considerable role of manganese-manganese exchange even at very low manganese concentration. This effect cannot be explained by only taking into account pairs of neighbouring manganese ions [12].

The exchange parameters α (for Γ_6) and β (for Γ_8) are estimated from the comparison between theory and experiments. The identification of f_{norm} with the Brillouin function for the alloy of $k = 0.0014$ allows the determination of βN_0

$$N_0\beta = 1.5 \text{ eV}, \qquad N_0\alpha = -0.75 \text{ eV}.$$

The signs of α (negative) and β (positive) imply that the spin splitting in both Γ_6 and Γ_8 Landau levels increases with the exchange interaction.

Experimental and theoretical transition energies are reported in figures (3-12) at $T = 4.2$ K and 2 K. The agreement between theory and experiments is excellent for most transitions in all investigated alloys at both temperatures. In particular, the theory fairly accounts for the curvatures of the lines. Population effects, discussed in section 7, explain the systematic discrepancies between theory and experiments for the transition $b_{\Gamma_6}(1) \rightarrow a_{\Gamma_8}(0)$ (Fig. 9, 11).

The knowledge of the band and exchange parameters enabled us to determine the eigenvalues and eigenvectors of the Landau levels, and therefore to estimate the relative oscillator strengths of the $\Gamma_6 \rightarrow \Gamma_8$ magnetooptical transitions. We checked that the dominant transitions are still given by the selection rules shown on table II.

6. Γ_8 **Landau levels spectrum.** — The Landau levels in Γ_8 bands are calculated, at $k_z = 0$, between 15 and 50 kG from the band parameters and the magnetization function (Fig. 19).

The field dependence of the energy, reported in figure 20, for several compositions at $T = 4.2$ and 2 K, exhibits interesting peculiarities resulting from the exchange effects.

As the spin interactions induce a shift (depend-

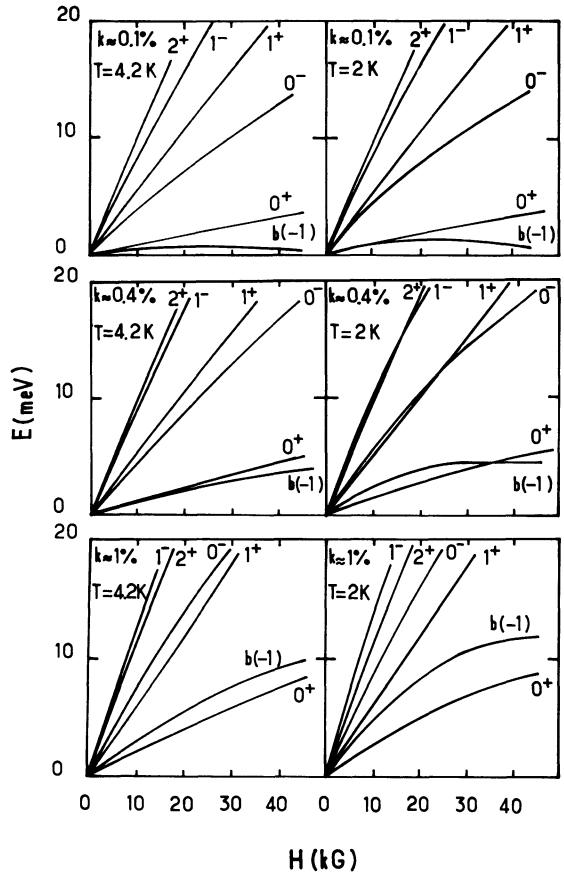

FIG. 20. — Magnetic field dependence of the Γ_8 Landau levels energy, at $k_z = 0$, for several compositions. $T = 4.2$ K and 2 K.

ing on k, H and T) of the Γ_8 energy levels (positive for $b(n)$, negative for $a(n)$, $n > 0$), the configuration of the spectrum is drastically modified with increasing Mn composition.

For $k = 0.0014$, the energy spectrum is distributed similarly to HgTe [10] and $Hg_{1-x}Cd_xTe$ alloys [7]; the main difference consists in the positive energy of the valence level $b(-1)$ and anomalous spin splitting of the electronic levels. With increasing k, the energies of the levels $a(n)$ and $b(n-1)$, shifted in opposite directions by the exchange effects, become very close for $k = 0.004$, but the spectrum conserves the same ordering.

For $k = 0.01$, the levels $b(n-1)$ overlap $a(n)$ which leads to an inverted disposition of the levels. In particular, the valence level $b(-1)$ overlaps the first electronic state $a(0)$.

By decreasing temperature, the magnetization effects are emphasized: The field-dependent shifts of $a(n)$ and $b(n)$ are more pronounced and the variations $E(H)$ exhibit curvatures reflecting the field dependence of the magnetization. This bowing effect is particularly remarkable on the hole level $b_{\Gamma_8}(-1)$ for which the contribution of the exchange interaction is predominant.

The energy of the valence level

$$\varepsilon_{b(-1)} = -\hbar\omega_0\left[\frac{1}{2}(\gamma_1 + \bar{\gamma}) - \frac{3}{2}\kappa\right] - 3A$$

presents a maximum, due to the saturation effect of $A(H)$, and then exhibits a decreasing field dependence. This behaviour implies a reduction of the overlap between $b_{\Gamma_8}(-1)$ and $a_{\Gamma_8}(0)$. For some particular composition, the crossing of $b_{\Gamma_8}(-1)$ and $a_{\Gamma_8}(0)$ occurs in the investigated field range which leads to a semimetal → semiconductor transition induced by the magnetic field. For $k = 0.004$, this semimetal → semiconductor transition occurs for $H = 37$ kG at $T = 2$ K.

The evolution with k of the lowest Landau levels described in figure 21 ($H = 30$ kG, $T = 2$ K) shows the overlaps between $a_{\Gamma_8}(0)$ and $b_{\Gamma_8}(-1)$ and the $b_{\Gamma_8}(0)$ and $a_{\Gamma_8}(1)$ level crossing.

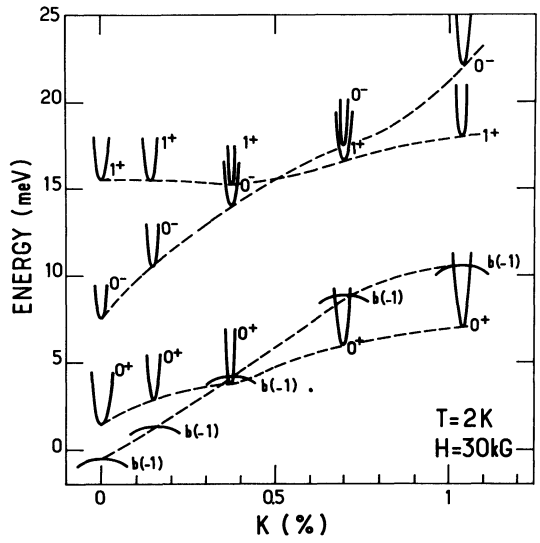

FIG. 21. — Evolution with the composition of the lowest Landau levels at $H = 30$ kG. $T = 2$ K.

The strong positive energy shift of the hole level $b_{\Gamma_8}(-1)$ is responsible for the occurrence of the intervalence transition $b_{\Gamma_6}(0) \rightarrow b_{\Gamma_8}(-1)$ in the σ^+ spectrum as the final state, merging from the Fermi level for alloys of composition $k \geqslant 0.004$, is depopulated. The existence of this additional and intense transition, systematically observed in the spectra of alloys with $k \geqslant 0.004$, constitutes a direct experimental evidence of exchange effects.

7. **Acceptor states and population effects.** — Similarly to HgTe and HgTe-CdTe alloys, HgTe-MnTe mixed crystals contain mercury vacancies which are partially reduced by annealing. These native defects acting as resonant acceptors in zero gap materials are experimentally revealed by the presence of impurity lines in magnetooptical spectra : transitions of elec-

trons from Γ_6 Landau levels to empty acceptor states are easily distinguishable from $\Gamma_6 \rightarrow \Gamma_8$ transitions :

— by the lineshape : they appear as broad structures due to the high density of acceptors (typically $N_A - N_D \sim 10^{16}$ cm^{-3}),

— by the field dependence of the energies : $\Gamma_6 \rightarrow A$cc transitions energies extrapolate to $\varepsilon_0 + \varepsilon_A$ whereas $\Gamma_6 \rightarrow \Gamma_8$ transitions converge to ε_0 at vanishing field. Figure 22 shows the impurity line $b_{\Gamma_6}(0) \rightarrow A$cc, observed for $\varepsilon /\!/ \mathbf{H}$ and σ^+ in the spectrum of sample A, beside the $\Gamma_6 \rightarrow \Gamma_8$ transitions $b_{\Gamma_6}(1) \rightarrow a_{\Gamma_8}(0)$ ($\varepsilon /\!/ \mathbf{H}$) and $b_{\Gamma_6}(1) \rightarrow b_{\Gamma_8}(0)$ (σ^+). From the knowledge of $b_{\Gamma_6}(0)$ energy we deduce the position of the acceptor state in the magnetic field : the binding

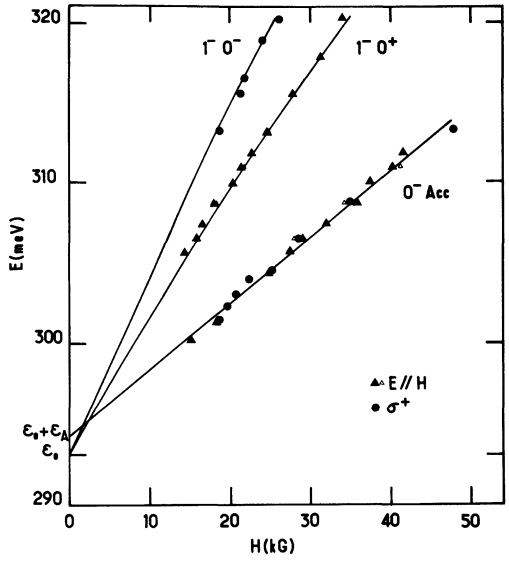

FIG. 22. — Energy versus H of the impurity ($b_{\Gamma_6}(0) \rightarrow A$cc) and lowest interband ($b_{\Gamma_6}(1) \rightarrow a_{\Gamma_8}(0)$, $b_{\Gamma_6}(1) \rightarrow b_{\Gamma_8}(0)$) transitions. Sample A. $T = 4.2$ K .

energy, about 1 meV, increases nearly linearly with H with a slope of 0.05 meV/kG. This result is comparable to the data obtained in $Hg_{1-x}Cd_xTe$ of low x. However, whereas $b_{\Gamma_6}(0) \rightarrow A$cc is systematically observed in zero gap $Hg_{1-x}Cd_xTe$ alloys, this transition only exists in the spectra of $Hg_{1-k}Mn_kTe$ mixed crystals of very low Mn content, namely for samples A and B. For k exceeding 0.008 (samples C, D, E), the impurity line disappears as the acceptor lies below the Fermi level in applied magnetic field. This population effect originates from the exchange interactions inducing a semimetallic configuration in the Γ_8 Landau spectrum : for such compositions, the heavy hole level $b_{\Gamma_8}(-1)$ lies in the electron continuum. As required by electrical neutrality, the Fermi level is tied to the valence level $b_{\Gamma_8}(-1)$ of high density of states.

The same population effect also explains the peculiar behaviour of the interband transition

$$b_{\Gamma_6}(1) \rightarrow a_{\Gamma_8}(0)$$

in the spectrum $\mathbf{E} /\!/ \mathbf{H}$. At $T = 4.2$ K, this line progressively weakens with increasing Mn content. By lowering the temperature from 4.2 K to 2 K, the intensity of the line decreases (this behaviour is illustrated on figure 23 for the sample C). For alloys D, E, the $b_{\Gamma_6}(1) \rightarrow a_{\Gamma_8}(0)$ transition is no longer observed at $T = 2$ K.

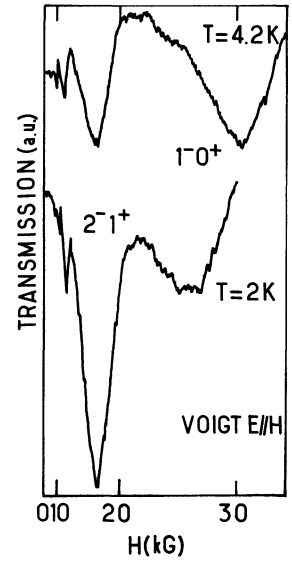

FIG. 23. — Temperature dependence between 4.2 K and 2 K of the lineshape at $\hbar\omega = 282.3$ MeV, sample C. Voigt geometry, $\varepsilon /\!/ \mathbf{H}$.

This temperature dependence of the intensity is connected with the filling of the $a_{\Gamma_8}(0)$ level. As shown on figure 23, the temperature decrease reduces the intensity of $b_{\Gamma_6}(1) \rightarrow a_{\Gamma_8}(0)$ but also shifts the position of the resonance line to lower field. This effect provides direct evidence of the location of the $a_{\Gamma_8}(0)$ edge below the Fermi level.

For sample C, whereas the transition occurs at $k_z = 0$ at $T = 4.2$ K, the population of $a_{\Gamma_8}(0)$ induces a Moss-Burstein shift of the resonance to $k_z \neq 0$ at $T = 2$ K. This effect is experimentally manifested by a reduction of the line strength, and also by a displacement to high energy of the resonance. This Moss-Burstein shift also explains the systematic discrepancies between the theoretical fits and experiments for the transitions $b_{\Gamma_6}(1) \rightarrow a_{\Gamma_8}(0)$ (Fig. 9, 11).

8. **Conclusion.** — The $\Gamma_6 \rightarrow \Gamma_8$ magnetooptical spectrum of semimetallic $Hg_{1-k}Mn_kTe$ alloys is quantitatively interpreted using the virtual crystal and molecular field approximations, and including exchange interactions in the framework of the Pidgeon and Brown model. The identical band structure for both alloy systems HgTe-CdTe, HgTe-MnTe of low composition ($-300 < \varepsilon_0 \leqslant -200$ meV) is proved by the same values of the band parameters. We show that the s-p and p-d exchange interactions are entirely responsible for the existence of striking

anomalies in $Hg_{1-k}Mn_kTe$ alloys which we have correlated to the spin dependent effects, e.g. anomalous gyromagnetic factors.

The theoretical model developed in the present study provides a relatively accurate determination of the exchange parameters and the magnetization function. The noticeable deviations from a Brillouin law invalidate the model of non interacting spins. Antiferromagnetic (at least predominantly) Mn-Mn correlations should be introduced to account for the experimental magnetization.

The Landau level energy spectrum in Γ_8, established at $k_z = 0$, exhibits quite pecular anomalies induced by the exchange interactions : the overlap of the levels $a_{\Gamma_8}(n)$ by $b_{\Gamma_8}(n-1)$ leads to a new ordering of the spectrum in alloys of $k > 0.004$. The overlap and the crossing of the highest valence $b_{\Gamma_8}(-1)$ and lowest conduction $a_{\Gamma_8}(0)$ give rise to a semimetal → semiconductor transition induced by the magnetic field.

The reorganization of the Landau level spectrum is expected to induce striking anomalies in all quantum phenomena.

References

[1] DELVES, R. T. and LEWIS, B., *J. Phys. Chem. Solids* **24** (1963) 549.

[2] BASTARD, G., RIGAUX, C., MYCIELSKI, A., *Phys. Status Solidi B* **79** (1977) 585.

[3] ANDRIANOV, G. D., GIMELFARB, F. A., KUSHNIR, P. I., LOPATINSKII, I. E., PASHKOVSKII, M. V., SAVELEV, A. S. and FISTUL, V. I., *Sov. Phys. Semicond.* **10** (1976) 66.

[4] HOLM, R. T. and FURDYNA, J. K., *Phys. Rev. B* **15** (1977) 844.

[5] LEIBLER, K., SIENKIEWICZ, A., CHECINSKI, K., GAŁASKA, R. R. and PAJACZKOWSKA, A., to be published in the Proceedings of the III International Conference on the Physics of Narrow-Gap Semiconductors, Warsaw, 1977.

[6] PIDGEON, C. R. and BROWN, R. N., *Phys. Rev.* **146** (1966) 575.

[7] GULDNER, Y., RIGAUX, C., MYCIELSKI, A., COUDER, Y., *Phys. Status Solidi B* **81** (1977) 615.

[8] GULDNER, Y., RIGAUX, C., MYCIELSKI, A., COUDER, Y., *Phys. Status Solidi B* **82** (1977) 149.

[9] KACMAN, P. and ZAWADZKI, W., *Phys. Status Solidi B* **47** (1971) 629.

[10] GULDNER, Y., RIGAUX, C., GRYNBERG, M. and MYCIELSKI, A. *Phys. Rev. B* **8** (1973) 3875.

[11] LUTTINGER, J. M., *Phys. Rev.* **102** (1956) 1030.

[12] DE SEZE, L., *J. Phys. C* **10** (1977) L-353.

[13] SAVAGE, H., RHYNE, J. J., HOLM, R., CULLEN, J. R., CARROLL, C. E. and WOHLFARTH, E. P., *Phys. Status Solidi B* **58** (1973) 685.

[14] KOSSUT, J., *Phys. Status Solidi B* **78** (1976) 537 ; Ph. D. Thesis, Institute of Physics, Polish Academy of Sciences (Warsaw, 1976).